THE JOURNAL OF BIOLOGICAL CHEMISTRY VOL. 283, NO. 15, pp. 9651–9658, April 11, 2008


# Solute Carrier 11 Cation Symport Requires Distinct Residues in Transmembrane Helices 1 and 6*[S]

Received for publication, December 4, 2007, and in revised form, January 18, 2008 Published, JBC Papers in Press, January 28, 2008, DOI 10.1074/jbc.M709906200

**Pascal Courville[‡], Eva Urbankova[§], Christopher Rensing[¶], Roman Chaloupka[§], Matthias Quick[‖], and Mathieu F. M. Cellier[‡1]**

*From the [‡]INRS-Institut Armand-Frappier, 531 Bd des prairies, Laval, Québec H7V 1B7, Canada, the [§]Faculty of Mathematics and Physics, Charles University, Institute of Physics, Ke Karlovu 5, 121 16 Prague 2, Czech Republic, the [¶]Department of Soil, Water, and Environmental Science, University of Arizona, Tucson, Arizona 85721, and the [‖]Center for Molecular Recognition, Columbia University, College of Physicians and Surgeons 11-401, New York, New York 10032*

**Ubiquitous solute carriers 11 (SLC11) contribute to metal-ion homeostasis by importing $Me^{2+}$ and $H^+$ into the cytoplasm. To identify residues mediating cation symport, *Escherichia coli* proton-dependent manganese transporter (MntH) was mutated at five SLC11-specific transmembrane (TM) sites; each mutant activity was compared with wild-type MntH, and the biochemical results were tested by homology threading. $Cd^{2+}$ and $H^+$ uptake kinetics were analyzed in whole cells as a function of pH and temperature, and right-side out membrane vesicles were used to detail energy requirements and to probe site accessibility by Cys replacement and thiol modification. This approach revealed that TM segment 1 (TMS1) residue $Asp^{34}$ couples $H^+$ and $Me^{2+}$ symport and contributes to MntH forward transport electrogenicity, whereas the TMS6 $His^{211}$ residue mediates pH-dependent $Me^{2+}$ uptake; MntH $Asn^{37}$, $Asn^{250}$, and $Asn^{401}$ in TMS1, TMS7, and TMS11 participate in transporter cycling and/or helix packing interactions. These biochemical results fit the LeuT/SLC6 structural fold, which suggests that conserved peptide motifs $Asp^{34}$-Pro-Gly (TMS1) and Met-Pro-$His^{211}$ (TMS6) form antiparallel "TM helix/extended peptide" boundaries, lining a "pore" cavity and enabling $H^+$-dependent $Me^{2+}$ import.**

Members of the natural resistance-associated macrophage protein (Nramp/SLC11) family (1, 2) are structurally conserved transporters catalyzing cellular uptake of redox metals such as $Fe^{2+}$ and $Mn^{2+}$. Mutations of *NRAMP1* orthologs in terrestrial vertebrates were linked to host phagocyte innate response to infections and immune diseases (3, 4). Genetic defects in *NRAMP2* (aka *DMT1*) affect iron homeostasis (intestinal absorption, erythropoiesis, and tissue distribution (2, 5, 6). Despite their medical importance, insight into the structure and function of SLC11 transporters is largely missing. Elucidation of the molecular mechanism underlying electrogenic $H^+$ and $Me^{2+}$ symport represents a milestone in the pursuit of future therapeutic approaches to treat $Me^{2+}$ homeostasis disorders, including brain diseases (7).

Prokaryotic orthologs of essential eukaryotic membrane transport functions represent attractive models to advance understanding of the mechanism of transport (8, 9). Studies from different groups showed that *Escherichia coli* proton-dependent manganese transporter (MntH)[2] is a valuable system for structure/function studies of $H^+$ and $Me^{2+}$ symport (10–13). MntH TM topology was established and selected mutations resulted in similar phenotypes in MntH and Nramp2 variants (6, 14, 15). In addition, *E. coli* MntH wild-type (WT) lacks cysteine residues, and site-directed introduction of Cys moieties combined to thiol modifications allows for detailed structural and functional mapping (16).

SLC11-dependent transport is typified by broad selectivity (*e.g.* $Mn^{2+}$, $Cd^{2+}$, $Fe^{2+}$, $Co^{2+}$, and $Ni^{2+}$) and $Me^{2+}$-specific interactions, including a range of $Me^{2+}/H^+$ stoichiometries depending on external conditions (10, 17–19). The $H^+$-dependent $Me^{2+}$ transport mechanism of eukaryotic Nramp homologs was deduced from studies of $Me^{2+}$ uptake and $Me^{2+}$-evoked currents, the external pH altering the transporter affinity for $Me^{2+}$ and the stoichiometry of $H^+$ and $Me^{2+}$ fluxes (2, 5). Kinetic models for $H^+$-coupled transport usually imply that $H^+$ binding or uptake depends at least partly on the membrane potential ($\Delta\psi$, and at high proton concentration (pH 5.5), large $Me^{2+}$-induced currents are mainly due to $H^+$ charge transfer across the membrane (17, 19).

To identify features defining the mechanism of transport of the SLC11 family, sites representing evolutionary type II rate shifts were targeted because they represent a radical shift in amino acid properties, which can contribute to functional divergence among homologous proteins including membrane proteins (20–22). Phylogenetic analyses distinguished the SLC11 family from a group of distantly related sequences (out-

* This work was supported in part by Canadian Institutes of Health Research Grant MOP-78014-MI (to M. C.), Czech Science Foundation Grant 204/07/0558 (to R. C.), and the Fondation Armand-Frappier (to P. C.). The costs of publication of this article were defrayed in part by the payment of page charges. This article must therefore be hereby marked "*advertisement*" in accordance with 18 U.S.C. Section 1734 solely to indicate this fact.

[S] The on-line version of this article (available at http://www.jbc.org) contains supplemental Figs. S1–S5, Table S1, and supplemental Methods 1 and 2.

[1] To whom correspondence should be addressed: INRS-Institut Armand-Frappier, 531, Bd des prairies, Laval, QC H7V 1B7, Canada. Fax: 450-686-5301; E-mail: mathieu.cellier@iaf.inrs.ca.

[2] The abbreviations used are: MntH, proton-dependent manganese transporter; F5M, fluorescein 5-maleimide; NEM, *N*-ethylmaleimide; RSOV, right-side out vesicles; ISOV, inside out vesicles; PMS, methylphenazonium methyl sulfate; Asc, ascorbate; CCCP, carbonyl cyanide *m*-chlorophenylhydrazone; Nramp, natural resistance-associated macrophage protein; SLC11, solute carrier 11; SLC6, solute carrier 6; TMS, transmembrane segment; LeuT, leucine transporter; EmrD, multidrug transporter EmrD; $\Delta\psi$, membrane potential; WT, wild type; Mes, 4-morpholineethanesulfonic acid; Pipes, 1,4-piperazinediethanesulfonic acid.

group <30% amino acid identity). Four type II rate shifts were identified at TM sites displaying polar or charged SLC11-specific amino acids matched by distinct outgroup-specific residues (10). Reciprocal residue exchange and additional mutations at each of these sites in TMS1, TMS6, and TMS11 were characterized, showing individual roles of each site in the $Me^{2+}$ and/or $H^+$ symport (10); among them residue $Asp^{34}$ appeared crucial for transport activity but its functional role remains undefined (10, 11).

The objective of this study was to elucidate the individual roles of the TM residues identified as evolutionary type II rate shift sites by analyzing the impact of the SLC11/outgroup reciprocal mutations on $Me^{2+}$ and $H^+$ uptake kinetics and thermodynamics *in vivo* and *in vitro*, by probing the *in situ* accessibility of targeted sites, and by selecting a tridimensional structural fold obtained by threading that fits our experimental results.

## EXPERIMENTAL PROCEDURES

*Site-directed Mutagenesis of E. coli MntH*—Site-directed mutagenesis was carried out as described previously (10). The oligonucleotide primers used to generate novel mutants are listed in supplemental Table 1. Mutant clones were selected by profiling *in vivo* $Me^{2+}$ sensitivity conferred upon expression in a metallo-dependent *E. coli* background (12). Full-length DNA sequence was determined for one clone of several that were functionally tested (CEQ 2000XL, Beckman Coulter, Mississauga, ON). The 12TMS-$His_{10}$ construct was generated by adding the 12th TMS of the *Lactobacillus casei* MntH C$\beta$1 homolog (23) and a $His_{10}$ tag. A StuI restriction site was introduced prior to the *mntH* stop codon to enable swapping of a StuI-XbaI flanked fragment of *mntH Cβ1* (residues 469–530, followed by a poly-His coding sequence).

*Fluorescent Measurements of H$^+$ Transport in Vivo*—Metal-induced intracellular acidification was measured using a pH-dependent ratiometric green fluorescent protein, pHluorin, and cells resuspended at an $A_{600}$ of 0.2 in 50 mM citrate-phosphate buffer (pH 4.7–5.7) (14). Fluorescence emission (wavelength 520 nm) was measured on a Fluoromax-2 spectrophotometer (Jobin-Yvon, SPEX) after dual excitation at 410 and 470 nm. MntH-dependent intracellular acidification was deduced from $[H^+]$ changes post-metal addition and monitored for 1000 s. Energy of activation ($E_a$) values were deduced from $[H^+]$ changes 250 s after addition of 10 $\mu$M $Cd^{2+}$ at temperatures varying from 15 to 37 °C.

*Preparation of Right-side Out and Inside Out Membrane Vesicles*—*E. coli* strain G536 (24) lacking several $Fe^{2+}$ and $Mn^{2+}$ transport systems (W3110 Δ*fecABCDE*::*kan* Δ*zupT*::*cat* Δ*mntH* Δ*entC* Δ*feoABC*) was transformed with derivatives of pBAD24 expressing native or mutant MntH. Individual clones were cultured in LB medium containing ampicillin (100 $\mu$g/ml) at 37 °C and 250 rpm until an $A_{600}$ of 0.6 was reached. MntH expression was induced for 1 h using 0.1% arabinose. Right-side out vesicles (RSOV) were prepared by osmotic lysis (25), except that spheroplasts were lysed in 0.1 M potassium $P_i$, pH 7.5, washed, and resuspended in 0.1 M Pipes-Mes, pH 7.5. Inside out vesicles (ISOV) were prepared by one passage of the cells (2.5 mg wet weight/ml) through an Aminco French Press at 16,000 p.s.i. in 0.1 M potassium $P_i$, pH 7.5, buffer (26). RSOV and ISOV were resuspended in 0.1 M Pipes-Mes, pH 7.5, at a concentration of 10–15 mg of protein/ml. The polarity of these preparations was tested by fluorescence spectrophotometry (supplemental Fig. S3) using indicators of (i) changes in $\Delta\psi$ or $\Delta$pH resulting from respiration (negative/alkaline or positive/acidic inside, respectively, for RSOV or ISOV), or (ii) topological accessibility of single Cys residues introduced in MntH extramembranous loops formerly assigned to either side of the membrane (14). These Cys mutants (MntH 12TMS-$His_{10}$) catalyzed $Cd^{2+}$-induced intracellular $H^+$ uptake (supplemental Fig. 3, *E* and *F*).

*$^{109}Cd^{2+}$ Transport Assays*—We used $Cd^{2+}$ as substrate for MntH because it triggers larger intracellular acidification compared with $Mn^{2+}$, $Fe^{2+}$, and $Co^{2+}$ (10). $^{109}$Cd (specific activity 60 mCi/$\mu$mol; GE Healthcare, Baie d'Urfé, Quebec, Canada) uptake was performed by a quick filtration assay in 0.1 (vesicles preparations) or 0.05 M Pipes-Mes (intact cells), pH 6.5 or 7.5, at 24 °C unless otherwise specified. Samples (0.1 ml) were removed at the indicated times and immediately filtered through 0.45-$\mu$m Metricel GN-6 filters (PALL, East Hills, NY; whole cells), 0.75-$\mu$m borosilicate GF75 microfiber filters (Advantec MFS Inc., Dublin, CA; RSOV), and 0.22-$\mu$m nitrocellulose filters (Whatman, Florham Park, NJ; ISOV). Filters were washed with 5 ml of ice-cold uptake buffer containing 1 mM $CdCl_2$. All experiments were performed at least in triplicate, using protein concentrations of 50 (RSOV), 200 (ISOV), and ~700 $\mu$g/ml (whole cells, corresponding to an $OD_{420}$ of 10) as determined by protein assay using a modified Lowry procedure (27). Vesicles were energized by adding 2 mM L-ascorbate and 0.02 mM *N*-methylphenazonium methyl sulfate (PMS/Asc), 10 mM D-lactate, or 5 mM NADH, for 3.5 min prior to the addition of $Cd^{2+}$. Ionophores (1 $\mu$M valinomycin, 0.1 $\mu$M nigericin, and 10 $\mu$M carbonyl cyanide *m*-chlorophenylhydrazone, CCCP) were added 1 min prior to PMS/Asc addition. $E_a$ (28) was measured using whole cells at pH 6.5 during the initial, linear phase of $Cd^{2+}$ uptake (after 10 s or 1 min) at temperatures varying from 24 to 37 °C. MntH specificity for $Mn^{2+}$ was verified using varying concentrations of $Mn^{2+}$ to compete $Cd^{2+}$ uptake. By fitting data to the Cheng-Prusoff equation, an apparent inhibitory constant, $K^i_{Mn} = 1.2 \pm 0.2$ $\mu$M at pH 6.5, and $[S] \sim K^{0.5}_{Cd} = 2.6 \pm 0.5$ $\mu$M $Cd^{2+}$, was obtained (29) (supplemental Fig. 1*A*), consistent with previous studies using $^{54}Mn^{2+}$ (13).

*Fluorescence Measurements of Membrane Potential ($\Delta\psi$) in RSOV and ISOV*—Fluorescent probes, 3,3′-dipropylthiadicarbocyanine iodide (1 $\mu$M) and bis-(1,3-dibutylbarbituric acid) pentamethine oxonol (1 $\mu$M), were used to monitor $\Delta\psi$ changes in energized vesicles as described (30). Fluorescence excitation and emission wavelengths were, respectively, 622 and 670 nm for 3,3′-dipropylthiadicarbocyanine iodide, and 588 and 614 nm for bis-(1,3-dibutylbarbituric acid)pentamethine oxonol. Measurements were performed either in 100 mM Pipes-Mes, 100 mM KCl, pH 7.5 (and 10 mM $CaCl_2$ or $MgSO_4$ in some cases), or 100 mM potassium $P_i$, 5 mM $MgSO_4$, pH 7.5. MntH electrogenicity was evaluated using RSOV (50 $\mu$g/ml proteins) energized with PMS/Asc (2/0.02 mM) and in the presence of 0.1 $\mu$M nigericin. Fluorescence changes indicating relative mem-

brane depolarization were recorded for 5 min post-addition of $Cd^{2+}$. 0.1 μM valinomycin was added finally as internal control.

*Site-directed Thiol Fluorescence Labeling*—Each MntH 12TMS-$His_{10}$ Cys derivative conferred *in vivo* $Me^{2+}$ sensitivity (supplemental Fig. 4*B*), consistent with respective data from prior mutagenesis (supplemental Fig. 2) (10), implying that Cys accessibility will reflect the functional structure of native MntH. RSOV (0.5 mg of protein) were labeled by incubation with 0.1 mM fluorescein 5-maleimide (F5M, Vector Laboratories, Burlingame, CA) at 23 °C for 10 min, prior to or after solubilization in detergent. When indicated RSOV were pretreated for 10 min with 0.5 mM 4-acetomido-4′-maleimidylstilbene 2,2′-disulfonic acid, disodium salt (Molecular Probes, Eugene, OR), or 0.5 mM *N*-ethylmaleimide (NEM) and then washed and resuspended or solubilized before labeling with F5M. ISOV (0.5 mg of proteins) were incubated for 5 min in the presence of 2.5 μM F5M; labeling was stopped by a 15-min incubation in 20 mM NEM. Membranes were solubilized, and the constructs purified as described under supplemental methods before SDS-PAGE (31) and Coomassie or silver nitrate staining (32). Prior to gel staining, F5M fluorescence was measured under a UV lamp equipped with a green filter using an Alpha Imager 3400 (Innotech, San Leandro, CA).

*Western Blot Analyses*—C-terminal tagged (-c-Myc or -12TMS-$His_{10}$) MntH variants were immunodetected in membrane preparations or in purified form as described (10) using anti-c-Myc (PerkinElmer Life Sciences) or anti-His (GE Healthcare) monoclonal antibodies.

*Homology Modeling*—Several approaches that use an alignment to map residues in a query sequence to sites in candidate template crystals structures were tested using the parameters specified by the developers, including Modeler (33), mGenThreader (34), and several others that are proposed on the meta-server LOMETS, including I-TASSER (9, 33, 35). Four sequences representative of the SLC11 family (two prokaryotic MntH and two eukaryotic Nramp) were tested and the results compiled to produce a consensus prediction. The PDB coordinates calculated were used visualize three-dimensional models using the freeware viewer PyMol (60). The root mean square deviation and *Z*-score of the LeuT models were verified using Combinatorial Extension (36), DaliLite (37), and MArkovian TRAnsition of Structure evolution (38).

## RESULTS

*Targeting Five Type II Evolutionary Rate Sites to Study the Mechanism of $Me^{2+}$ and $H^+$ Symport*—The functional impact of mutating four SLC11-specific TM sites (MntH $Asp^{34}$, $Asn^{37}$, $His^{211}$, and $Asn^{401}$; Ref. 10) suggested that further kinetic and thermodynamic analyses of mutants at these sites would inform understanding of structure-function relationships. We thus studied mutants in which the SLC11 residues were exchanged for the matching outgroup moiety. The presence of two Asn residues at selected sites suggested also include MntH TMS7 $Asn^{250}$, which is invariant in the SLC11 family and substituted for Thr or Ser in the outgroup. Because replacement of MntH $Asn^{401}$ with Thr produces a phenotype similar to the exchange for the matching outgroup moiety (Gly) (10), we analyzed MntH mutants N37T, N250T, and N401T. The TM location of the targeted sites is schematized (Fig. 1*A*) based on previous predictions and experimental determinations (11, 14, 15, 39). The mutant proteins displayed membrane expression levels similar to MntH-WT, indicating that the substitutions were structurally well tolerated (Fig. 1*B*).

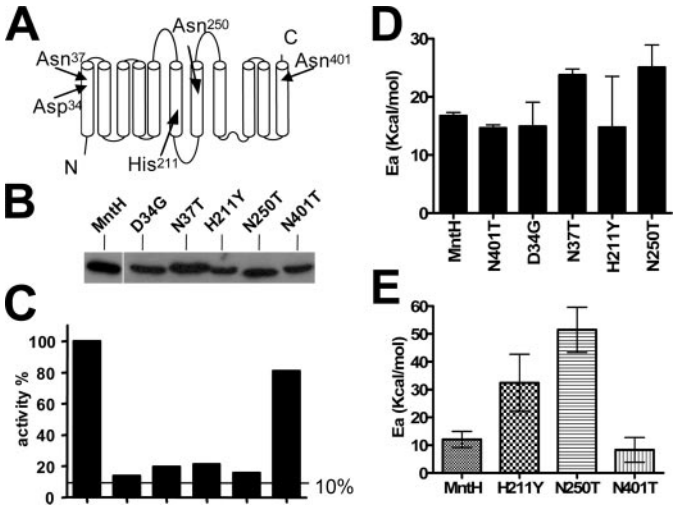


FIGURE 1. **Thermal activation of *E. coli* MntH mutants activity.** *A*, low resolution *E. coli* MntH topological model. *Arrows* indicate the predicted location of MntH residues corresponding to SLC11-specific sites. *B*, Western blot of c-Myc-tagged mutants (80 μg of membrane proteins/lane). *C*, $Cd^{2+}$ uptake by *E. coli* GR536 cells expressing MntH-WT and -mutants at SLC11 type II evolutionary sites. Uptake of 10 μM $^{109}Cd^{2+}$ (60 mCi/μmol) was measured for 10 s at 37 °C, pH 6.5. *D* and *E*, Arrhenius $E_a$ plots of MntH activity (15–37 °C) deduced using the equation $k = A \times \exp^{(-E_a/RT)}$, where *k* is the rate coefficient, *A* is a constant, *R* the universal gas constant and *T*, temperature in K, for $Cd^{2+}$ uptake quantified by radio-filter assay (*D*), and $Cd^{2+}$-induced $H^+$ uptake measured by ratiometric fluorescence analysis of intracellular pH (*E*).

**TABLE 1**
**Kinetics of MntH $Cd^{2+}$ transport in whole cells at pH 6.5 and 7.5**

Data obtained at 37 °C in 0.05 M Pipes-Mes and 10 s after addition of $^{109}Cd^{2+}$ is shown.

| MntH | $K^{0.5}_{Cd}$ | | $V_{max}$ | |
|---|---|---|---|---|
| | pH 6.5 | pH 7.5 | pH 6.5 | pH 7.5 |
| | μM | | *nmol/min* | |
| Wild-type | 2.6 ± 0.5 | 9.1 ± 2.9 | 13.4 ± 2.1 | 31.2 ± 4.6 |
| D34G[a] | 21.1 ± 3.6 | 32.0 ± 9 | 10.4 ± 0.7 | 8.1 ± 0.3 |
| N37T[a] | 15.0 ± 2.5 | 43.0 ± 15 | 9.7 ± 0.3 | 10.0 ± 3.0 |
| H211Y[a] | 4.4 ± 1.1 | NA[b] | 4.3 ± 0.3 | NA |
| N250T[a] | 4.3 ± 0.1 | 12.5 ± 0.8 | 3.7 ± 0.1 | 3.5 ± 0.4 |
| N401T | 2.1 ± 0.6 | 10.4 ± 0.8 | 7.7 ± 0.7 | 28.2 ± 0.9 |

[a] Data collected 1 min, pH 6.5, and 2 min, pH 7.5, after addition of $^{109}Cd^{2+}$.
[b] NA, not applicable (similar to Δ*mntH* cells).

*Characterization of E. coli MntH $Cd^{2+}$ and $H^+$ Transport in Vivo*—To study the effects of the external pH on the kinetics of MntH, we measured $^{109}Cd^{2+}$ uptake and $Cd^{2+}$-dependent intracellular acidification in intact *E. coli* cells. $Cd^{2+}$ uptake by MntH-WT (Fig. 1C) revealed $K^{0.5}_{Cd}$ values at 37 °C of 2.6 ± 0.5 μM at pH 6.5 and 9.1 ± 2.9 μM at pH 7.5 (data fitted to the Michaelis-Menten equation, Table 1). The maximal velocity ($V_{max}$) of $Cd^{2+}$ transport was lower at pH 6.5 compared with pH 7.5. MntH-catalyzed $Cd^{2+}$-induced $H^+$ uptake was activated by increasing amounts of $Cd^{2+}$, with $K_{0.5}$ values at 23 °C ranging from 0.78 to 1.4 μM $Cd^{2+}$ (pH 4.7–5.7, respectively, Table 2 and supplemental Fig. 1, *B* and *C*). In both systems, lowering the external pH increased MntH affinity for $Cd^{2+}$.

To discriminate carrier-type from channel-mediated transport the Arrhenius $E_a$ values were measured (28, 40) for $Cd^{2+}$

**TABLE 2**

**Kinetics of MntH $Cd^{2+}$-induced intracellular acidification at pH 4.7 and 5.3**

Data were obtained at 23 °C in 50 mM citrate-phosphate buffer and 1000 s after addition of $Cd^{2+}$.

| MntH | $K_{0.5}$ | | $V_{max}$ | |
|---|---|---|---|---|
| | pH 4.7 | pH 5.3 | pH 4.7 | pH 5.3 |
| | μM | | pM/s | |
| Wild-type | 0.8 ± 0.2 | 1.4 ± 0.3 | 98 ± 6 | 34 ± 2 |
| D34G | NA[a] | NA | NA | NA |
| N37T | NA | NA | NA | NA |
| H211Y | 30 ± 9 | 500 ± 300 | 116 ± 9 | 28 ± 7 |
| N250T | 140 ± 10 | 40 ± 20 | 81 ± 8 | 18 ± 2 |
| N401T | 4 ± 1 | 5 ± 2 | 190 ± 20 | 101 ± 7 |

[a] NA, not applicable (D34G, no activity; N37T, $K_{0.5}$ ~ 600 μM at pH 4.7).

uptake and $Cd^{2+}$-induced intracellular acidification. $E_a$ values (Fig. 1, *D* and *E*) were in the range of those obtained for carriers (10.7–26.3 kcal/mol, *versus* channels, 4.3–8.1 kcal/mol) supporting the notion of MntH transport cycle and intramolecular structural rearrangement. This could involve for instance, an external open conformation loading $Me^{2+}$ and $H^+$ to translocate them to the inner face of the membrane, before unloading and then rapidly back-translocating to reload (16).

MntH $Cd^{2+}$ uptake activity was drastically reduced for four of the mutants studied (Fig. 1*C*). Further analyses of MntH $Cd^{2+}/H^+$ symport kinetics and thermodynamics revealed various types of effects (Tables 1 and 2), which can be summarized as: (i) low affinity $Me^{2+}$ uptake and little $H^+$ transport (Asp$^{34}$ and Asn$^{37}$), (ii) reduced $Me^{2+}$ uptake but significant residual $H^+$ uptake (Asn$^{250}$, His$^{211}$), or (iii) slight opposite variations in $Cd^{2+}$ and $H^+$ uptake (Asn$^{401}$), and (iv) impaired transporter cycling (Asn$^{37}$, Asn$^{250}$, and His$^{211}$). Individual phenotypes are detailed below.

*MntH TMS1 Asp$^{34}$ Is Essential for Coupling H$^+$ and Cd$^{2+}$ Uptake*—Kinetic analyses of the MntH-D34G mutant revealed dose-dependent $Cd^{2+}$ uptake, and $K_{Cd}^{0.5}$ values that were increased about 2- and 10-fold compared with MntH-WT at pH 7.5 and 6.5, respectively, but $Cd^{2+}$-induced $H^+$ uptake was not detected even when using 1 mM $Cd^{2+}$ (supplemental Fig. 2*D*). The unique properties of the MntH-D34G mutant, such as $K_{Cd}^{0.5}$ values little affected by the external pH and lack of $H^+$ transport, suggested that exchange of Asp$^{34}$ uncoupled $Cd^{2+}$ uptake from $H^+$ influx.

To determine whether a conformational rearrangement was involved we tested the $E_a$ of $Cd^{2+}$ uptake by MntH-D34G, which was similar to MntH-WT (Fig. 1*D*). The $E_a$ of $H^+$ uptake could not be measured because no significant activity was detected for any Asp$^{34}$ variant (supplemental Fig. 2*D*). This indicated that mutation of Asp$^{34}$ could directly affect $H^+$ binding *versus* transporter cycling, which was confirmed *in vitro* by lack of a $Cd^{2+}$-induced MntH-dependent variation of $\Delta\psi$ in right-side out vesicles (see below "Electrogenicity of MntH-dependent Forward $Cd^{2+}$ Transport " and Fig. 3*E*).

*MntH TMS6 His$^{211}$ Role in Cd$^{2+}$ Transport is pH-dependent*—The exchange of TMS6 His$^{211}$ for Tyr had pH-dependent effects on MntH $Cd^{2+}$ uptake. Compared with MntH-WT, the $K_{Cd}^{0.5}$ value of MntH-H211Y doubled at pH 6.5, but at pH 7.5, $Cd^{2+}$ uptake levels were indistinguishable from cells lacking a functional MntH (Table 1). At pH 6.5, the MntH-H211Y $V_{max}$ value was reduced (Table 1), and the $E_a$ value possibly affected (Fig. 1*D*). Similar strongly pH-dependent $Me^{2+}$ uptake activity has been reported for Nramp2 mutation at the homologous site, H267A, which was compensated for by lowering the external pH (41).

To examine whether this SLC11 invariant His residue is crucial for pH-dependent $Me^{2+}$ binding we measured $Cd^{2+}$-induced variations in intracellular pH (Table 2, supplemental Fig. 1, *B* and *C*). The apparent $K_{0.5}$ of MntH H211Y was several 100-fold increased at pH 5.3 compared with WT. The $V_{max}$ value for $H^+$ accumulation showed that this mutant still catalyzed $H^+$ uptake, although the $E_a$ value of $H^+$ transport was elevated (Fig. 1*E*). The results thus indicated that replacement of MntH TMS6 His$^{211}$ alters $H^+$ binding and the catalytic cycle of $Cd^{2+}$ binding and transport.

*MntH Asn$^{37}$, Asn$^{250}$, and Asn$^{401}$ Contribute Indirectly to Cotransport Activity*—The MntH Asn$^{250}$ mutant also showed unique effects compared with MntH-WT: up to an 100-fold increase in the apparent $K_{0.5}$ value for $Cd^{2+}$-induced $H^+$ uptake at pH 4.7 and reduced $V_{max}$ values (Table 2 and supplemental Fig. 1, *B* and *C*); strong reduction in the $V_{max}$ values for $Cd^{2+}$ uptake, especially at pH 7.5 and a lesser increase of $K_{Cd}^{0.5}$ values, mainly at pH 6.5 (Table 1); and elevated $E_a$ values of both $Cd^{2+}$ and $H^+$ transport (Fig. 1, *D* and *E*). Because N250Q exchange was not conservative (compared with N401Q, supplemental Fig. 2) these results indicated a role of Asn$^{250}$ in transporter cycling.

Although replacement of Asn$^{37}$ affected $Cd^{2+}$ and $H^+$ transport kinetics similarly to Asp$^{34}$ mutation, maybe due to proximity of these sites, important differences were noted: the MntH-N37T mutation did not abrogate $Cd^{2+}$-induced $H^+$ uptake (supplemental Fig. 2*D*), whereas the $E_a$ value of $Cd^{2+}$ transport was elevated (Fig. 1*D*), and $K_{Cd}^{0.5}$ values remained pH-dependent (Table 1). The MntH Asn$^{37}$ residue may, similarly to Asn$^{250}$, take part in conformational changes during the transport cycle.

MntH mutation Asn$^{401}$ to Thr had less impact on transport kinetics than N37T and N250T exchanges (Fig. 1), consistent with Asn to Gln replacement that was conservative only at site 401 (supplemental Figs. 1 and 2). Main effects were on MntH-N401T $V_{max}$, which was reduced for $Cd^{2+}$ uptake especially at pH 6.5 (Table 1), but increased ~2-fold for $Cd^{2+}$-induced $H^+$ uptake, independent of the external pH (Table 2, supplemental Fig. 1, *B* and *C*). pH-dependent variations of $K_{Cd}^{0.5}$ were not correlated with $Cd^{2+}$ transport $V_{max}$ values. Such effects supported previous observations linking nonconservative mutations of Asn$^{401}$ to intracellular acidification in the absence of added $Cd^{2+}$ (10), due to apparently opposite effects on the $V_{max}$ values of $Me^{2+}$ and $H^+$ uptake.

*Characterization of MntH-catalyzed Forward Metal Uptake in Vitro*—To confirm the uncoupling effect of the MntH D34G mutation observed *in vivo* we studied $Cd^{2+}$ transport *in vitro* using RSOV. ISOV were used for comparison. MntH-dependent $^{109}Cd^{2+}$ uptake in 0 trans conditions showed different requirements for RSOV or ISOV preparations (Fig. 2, *A* and *B*). Uptake into RSOV was stimulated about 10-fold of the background levels by addition of millimolar amounts of $Ca^{2+}$ and the respiratory substrate PMS/Asc (42), whereas 10-fold more metal was necessary to obtain about 3-fold stimulation of back-

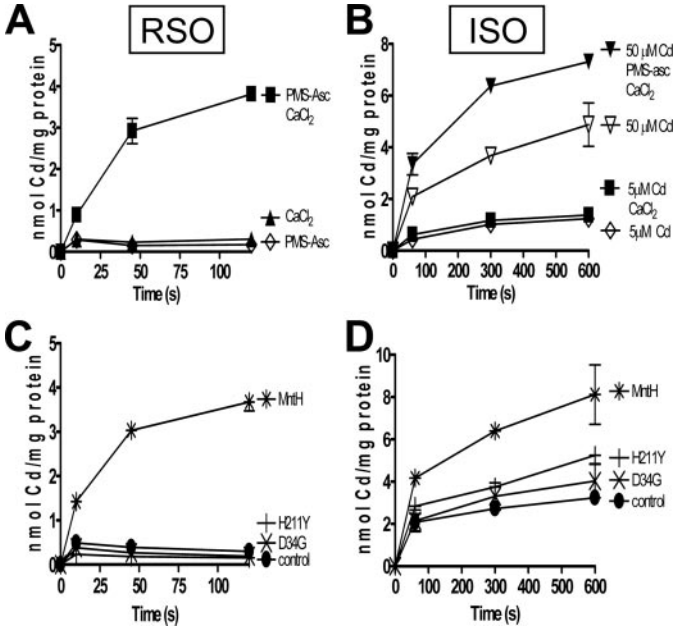


FIGURE 2. **MntH-dependent $Cd^{2+}$ transport in vesicles of correct and inverted orientations.** $Cd^{2+}$ uptake was measured in right-side out vesicles (RSOV, *A* and *C*) and inside out vesicles (ISOV, *B* and *D*) using, respectively, 5 or 50 $\mu$M $^{109}Cd^{2+}$ (60 mCi/$\mu$mol) in 0.1 M Pipes-Mes, pH 6.5, and PMS/Asc as respiratory substrate where indicated, in the presence or absence of 10 mM $CaCl_2$. Control values, vesicles harboring no MntH protein. *A* and *B*, transport by MntH-WT was performed as described under "Experimental Procedures"; control values were subtracted. *C* and *D*, forward and reverse $Cd^{2+}$ transport by MntH-WT, -D34G, and -H211Y.

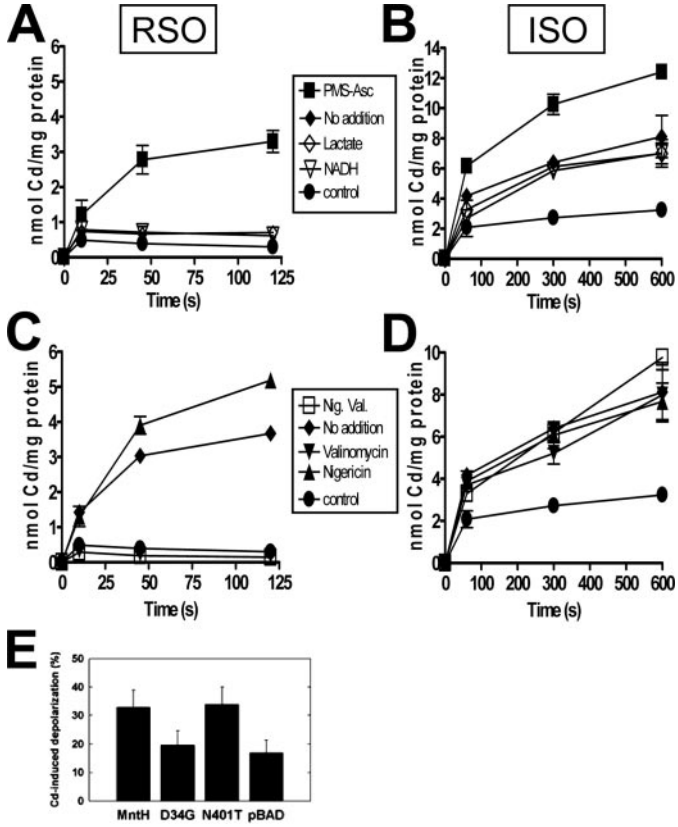


FIGURE 3. **Energy requirements and electrogenicity of MntH $Cd^{2+}$ uptake.** Time course of transport was measured at 23 °C, pH 6.5, with 5 $\mu$M $Cd^{2+}$ (RSOV; *A* and *C*) or 50 $\mu$M $Cd^{2+}$ (ISOV; *B* and *D*). Vesicles were preincubated with respiratory substrates (*A* and *B*) or $K^+$ and/or $H^+$ ionophores (*C* and *D*, in presence of 0.1 M KCl) before measuring transport by radiofilter assay. *Control*, vesicles harboring no MntH protein. *E*, MntH-dependent depolarization of $\Delta\psi$ induced in RSOV by addition of $Cd^{2+}$ and measured as described in supplemental Methods. Mean ± S.E. of 7–14 replicas; *pBAD*, vector control.

ground uptake in ISOV (Fig. 2, *A* and *B*). However, both $Cd^{2+}$ uptake activities were saturable, temperature-dependent (data not shown), and required an active transporter: mutants at sites thought to interact directly with $Cd^{2+}$ and $H^+$ showed little uptake in conditions otherwise favorable for MntH-WT (Fig. 2, *C* and *D*).

MntH uptake in RSOV was stimulated by a potent electron donor (PMS/Asc *versus* lactate or NADH, Fig. 3*A*). In the presence of 1 unit of ΔpH (10-fold variation in $[H^+]$), $Cd^{2+}$ uptake was increased by adding the $H^+/K^+$ ionophore nigericin, which converts ΔpH into increased $\Delta\psi$ (43), and it was abrogated using the $K^+$ ionophore valinomycin, which dissipates $\Delta\psi$ (Fig. 3*C*). Without external $K^+$, $Cd^{2+}$ transport still required PMS/Asc and $Ca^{2+}$ but was not affected by nigericin, slightly stimulated with valinomycin, and the protonophore CCCP abrogated it (data not shown). Thus, MntH forward $Me^{2+}$ uptake activity is proton-dependent.

In contrast, and contrary to the expected inhibition by $\Delta\psi$ (positive inside) of a proton-motive force-dependent mechanism of $Cd^{2+}$ uptake, MntH-dependent activity in ISOV persisted in the presence of 10 mM D-lactate or 5 mM NADH (Fig. 3*B*) and was indifferent to nigericin, valinomycin, or both as well as up to 100 $\mu$M CCCP (Fig. 3*D*). Also, compared with RSOV, PMS/Asc and $Ca^{2+}$ induced little stimulation of $Cd^{2+}$ uptake in ISOV, which was nullified by CCCP (consistent with ~90% homogeneous ISOV preparations, supplemental Fig. 3*D* and data not shown). These data distinguished MntH "reverse " transport from proton-dependent forward transport activity.

*Electrogenicity of MntH-dependent Forward $Cd^{2+}$ Transport*—Observation of $Me^{2+}$ uptake driven by $\Delta\psi$ only (negative inside) into RSOV preparations (Fig. 3*C*) was consistent with *in vivo* data (supplemental Fig. 4*A*) using an *E. coli* Δ*unc* strain, unable to convert ATP and the proton-motive force, in which MntH $Mn^{2+}$ uptake at pH 7.4 (ΔpH ~ 0) was independent of ATP and abrogated by micromolar amounts of CCCP. These data suggested that MntH forward transport activity, symporting $Me^{2+}$ and $H^+$, is electrogenic, *i.e.* it produces charge imbalance across the membrane.

Consequently, MntH activity should contribute directly to modulate $\Delta\psi$; using conditions where RSOV are energized with $\Delta\psi$ only (negative inside), MntH-dependent symport of $Me^{2+}$ and $H^+$ should in turn reduce $\Delta\psi$. Such MntH-dependent charge movement across the membrane was quantified by following $Cd^{2+}$-induced depolarization of $\Delta\psi$. Because addition of 100 $\mu$M $Cd^{2+}$ to RSOV harboring MntH-D34G yielded low level $Cd^{2+}$ uptake at pH 6.5 (data not shown), this concentration was used to follow the $Cd^{2+}$-induced variation in $\Delta\psi$ (less negative inside). Similar depolarization was observed with the MntH-WT and -N401T mutants (Fig. 3*E*), reflecting electrogenic, non-compensated charge movement across the vesicle membrane. Deficient electrogenicity of MntH-D34G supported the loss of the $Cd^{2+}$-induced $H^+$ symport in this mutant.

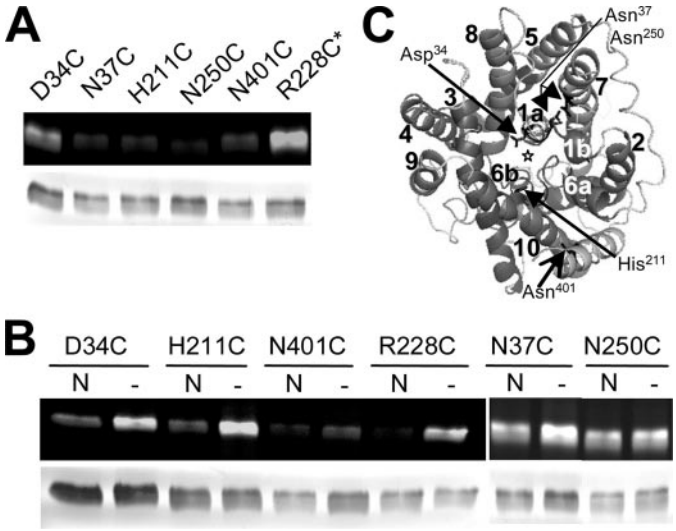


FIGURE 4. **Topological accessibility of MntH TMS1 Asp[34] and TMS6 His[211].** *A* and *B*, *in situ* accessibility of single cysteine residues introduced in MntH 12TMS-$His_{10}$ at either SLC11-specific sites or the control cytoplasmic site 228 (supplemental Fig. 3) was assayed using RSOV. *Top panel*, in-gel F5M fluorescence was visualized under UV; *bottom panel*, silver nitrate staining of the corresponding $Ni^{2+}$ affinity purified proteins. *In situ* accessibility was revealed by direct labeling with F5M (*A*; except *, labeling after solubilization), or reaction with NEM (*N*) or not (−) before solubilization and F5M labeling (*B*), as described under "Experimental Procedures." *C*, view from the periplasm of the LeuT-based SLC11 model obtained by threading. Half-helices 1a and 6b are placed at the *bottom*, orthogonal to the membrane plan; sites comprising the top "*loop EL4*" (44) are not shown for clarity. Positions predicted for cation binding sites Asp[34] and His[211], close to the center (indicated by *star*), and for the other sites studied are indicated by *arrows*. *Numbers 1–5* and *6–10* designate the TMS forming the inverted domains.

*MntH Asp[34] and His[211] Are Accessible to Solvent and Predicted to Line a Permeation Pathway*—Direct involvement of Asp[34] in coupled $Cd^{2+}$ and $H^+$ uptakes suggested that this residue could interact with either cation through a water-filled "pore," and should thus be solvent-accessible. To address this possibility, single Cys mutants were produced using a MntH construct that had been modified to add a 12th TMS and a C-terminal cytoplasmic His tag that allowed affinity purification. The MntH 12TMS-$His_{10}$ construct exhibited transport activity similar to MntH-WT (supplemental Figs. 3*F* and 4*B*). RSOV harboring each of the MntH single Cys mutants at the five Nramp/SLC11-specific sites (34, 37, 211, 250, and 401) were probed *in situ* with sulfhydryl reagents, either bulky and polar, F5M, or small and permeable, NEM.

Strikingly, only two sites were reachable *in situ*: Cys[34] was freely accessible to F5M (Fig. 4*A*) and Cys[211] reacted solely with NEM (Fig. 4, *A* and *B*). These results seemed consistent with the Asp[34] and His[211] respective predicted locations in TMS1 and TMS6 and their distinct direct roles in $Me^{2+}/H^+$ symport. Also, TMS1 Cys[37] and TMS7 Cys[250] became labeled with F5M after solubilizing MntH (Fig. 4, *A* and *B*), supporting possible roles in the transporter motion. TMS11 Cys[401] was marginally accessible (Fig. 4, *A* and *B*) implying that it participates to tight inter-helical contacts; exchanging Asn[401] for a smaller side chain increased cation uptake, whereas a similar sized moiety limited it (*e.g.* supplemental Fig. 4*B* and 2, *A* and *C*, respectively, Cys and Gln; prior data using Gly and Thr, see Ref. 10). The results of site-directed labeling thus converged with functional data to demonstrate that SLC11-specific residues contribute critically to MntH transport by either binding substrates directly (Asp[34], His[211]) or contributing to inter-helices contacts (Asn[37], Asn[250], and Asn[401]).

Three-dimensional mapping of functional sites is crucial to understand catalytic mechanisms. We determined whether known transporter structures could help model a spatial distribution for the SLC11-specific functional sites. Several template structures, *e.g.* LeuT, glycerol-3-phosphate transporter, EmrD, and chloride channel, were frequently ranked as significant hits with most programs and for each SLC11 sequence tested. However, only the LeuT/SLC6 family structure (44) fully supported our functional and topological data (Fig. 4*C* and supplemental Fig. 5). Additional predictions obtained using Modeler and either single sequences or groups of sequences representing SLC11 phylotypes as queries produced 16 models, which were all based on the LeuT template, and with scores ranging from 0.01 to 0.76. The similarity of each of these models with the LeuT structure was quantified using DaliLite (37) yielding values in the ranges 44–60.3 (*Z*-score), 322–439 (aligned residues), 0.8–1.7 (Å, root mean square deviation), and 10–17 (% sequence identity), which indicated that SLC11 transporters may share the same general fold. The model presented (Fig. 4*C*; supplemental Fig. 5) exhibits little difference with the LeuT/SLC6 structure, with values for root mean square deviations and *Z*-score of, respectively, 1.07 Å and 7.5 (45) or 1.0 Å and 52.9 (37). This LeuT fold places both Asp[34] and His[211] in the inner core of the MntH molecule, as parts of extended peptides interrupting TMS1 and TMS6, and lining a water-filled pore. The three Asn[37], Asn[250], and Asn[401] appeared directed toward inter-helix contacts and the outer fence of the model architecture (Fig. 4*C* and supplemental Fig. 5). Structural modeling of SLC11 evolutionary distinct sites thus corroborates their key functional roles.

## DISCUSSION

The present study showed that MntH Asp[34] and His[211], two SLC11 family-specific and ionizable residues located in TMS1 and TMS6 are necessary for binding and transport of $H^+$ and $Me^{2+}$. Whereas interdependent transport of $Me^{2+}$ and $H^+$ by MntH is consistent with properties reported for eukaryotic Nramp homologs (17, 46), we demonstrated here for the first time that exchange of MntH TMS1 Asp[34] uncoupled $H^+$ and $Cd^{2+}$ transport and also reduced affinity for $Cd^{2+}$, but preserved pH-independent $Cd^{2+}$ uptake and transporter cycling. Because this site was also freely accessible *in situ*, it is likely part of an $H^+$ translocation pathway. Exchange of MntH TMS6 His[211] rendered affinity for $Cd^{2+}$ more dependent on the external pH but preserved $Cd^{2+}$-induced $H^+$ transport; Cys[211] was accessible *in situ* only to a small reagent, supporting a direct role of His[211] (de)protonation in $Cd^{2+}$ transporter cycling. The SLC11-specific TMS1 Asp and TMS6 His residues constitute thus functional determinants of $Me^{2+}$ and $H^+$ symport.

The TMS1 Asp residue is part of a conserved DPGN motif that has been subjected to mutagenesis in studies using MntH or Nramp2 homologs, which showed loss of $Me^{2+}$ uptake caused by Gly exchange (11, 47). The carboxyl end of Nramp2 TMS1 and adjacent extra loop were implicated in $Me^{2+}$ binding and coupling of $Me^{2+}$ uptake to the proton-motive force

(47). MntH scanning mutagenesis revealed that only Pro$^{35}$ exchange did not abrogate $Mn^{2+}$ uptake, and MntH-P35G had a marginally affected $K^{0.5}_{Mn}$ (11). Here, the role of the flanking SLC11 family-specific site Asn$^{37}$ was detailed. Exchange of Asn$^{37}$ seemed to perturb interactions among TMS rather than between MntH and cations, as demonstrated by inaccessibility to a small soluble compound *in situ*, impaired $Cd^{2+}$ and $H^+$ transporter cycling but residual $Cd^{2+}$-induced $H^+$ transport, and pH dependence of $Cd^{2+}$ uptake. We deduce that the SLC11 invariant tripeptide (DPG) may bear analogy to a known functional signature for $Me^{2+/+}$ transport, *i.e.* ((C/S/T)P(C/H)) that is conserved in the TMS6 of $P_{1B}$-type ATPases, which pump heavy metal cations using energy provided by ATP hydrolysis (48, 49). The SLC11-invariant Asp and Gly residues in TMS1 could thus contribute to $Me^{2+}$ binding, the acidic moiety being key for $H^+$-coupled transport.

The His residue in TMS6 was shown previously to regulate $Me^{2+}$ uptake via Nramp2 and MntH (10, 41). We further showed that low $Me^{2+}$ uptake persisted with MntH-H211C (supplemental Fig. 4*B*), similar to the Nramp2 matching mutant H267C (41), and that MntH-H211Y low affinity for $Cd^{2+}$ did not prevent $H^+$ uptake. It seems thus unlikely that this His residue could either bind $Me^{2+}$ directly, or simply be part of a relay or channel enabling $H^+$ movement across the membrane (50, 51). Instead, (de)protonation could favor a conformation facilitating $Me^{2+}$ translocation and transporter cycling; TonB His$^{20}$ is an example of a TM His moiety required for transport cycling and the energy transduction event (52). The SLC11-specific TMS6 His residue is part of another conserved motif (MPH) (with exceptions in plasmodia, plants, and fungi homologs) not found in the SLC11 phylogenetic outgroup (V(P/G)Y) (10), suggesting by analogy with TMS1 that the TMS6 motif (MPH) may represent another signature for metal transport.

Strikingly, modeling SLC11 homologs on the LeuT/SLC6 structure suggests an internal symmetry (including two domains made of helices 1–5 and 6–10, similarly folded but in inverted orientation with respect to the membrane (53), and thus a possible origin for the motifs in TMS1 and TMS6, which appear central to the model transporter architecture. These two motifs in anti-parallel orientation ((DPG) and ("HPM")) form a pair of extended peptides interrupting TMS1 and TMS6. Similar pairs of discontinuous helices ($\alpha$-helix-extended peptide-$\alpha$-helix) constitute a salient feature in five cation transporter structures, and pairs of antiparallel discontinuous TM helices may be part of a fold shared by several cation transporter families (54).

Burying such (DPG) and (HPM) "extended peptides/polar helix termini" elements within the low-dielectric core of the membrane is not energetically favored, partly due to charges, including polar backbone groups not engaged in intra-chain hydrogen bonds. Such elements should be stabilized by interacting with adjacent residues, transported substrates (*e.g.* dehydrated cations), or by mediating alternate conformation rearrangements (44, 54). Our data indicate that interactions with $Me^{2+}$ and/or $H^+$ may stabilize SLC11 TMS1 Asp and TMS6 His. Mapping to the LeuT model are other sites of potential divergence between the SLC11 family and outgroup, suggested clustering around these central motifs, (DPG) and (HPM) (supplemental Fig. 5, *C* and *D*), and possible inter-helix contacts, which could be considered in future structure/function studies using the present approach. The targeted Asn residues in TMS1, TMS7, and TMS11 affected transport without interacting with cations or being accessible to NEM *in situ* (Asn$^{37}$, Asn$^{250}$, and Asn$^{401}$). According to the LeuT fold, these residues may be oriented for inter-helix contacts, possibly key for transport cycling, *e.g.* TMS7 Asn$^{250}$ and TMS1b Asn$^{37}$, or velocity (Asn$^{401}$), because TM Asn residues can drive strongly inter-helix associations (55, 56) or mediate structural motion during ion permeation (57).

Analysis of *E. coli* MntH activity *in vitro* yielded surprising results concerning activation of MntH forward $Cd^{2+}$ transport by millimolar amounts of $Ca^{2+}$, and reverse $Cd^{2+}$ transport that appeared passive. Requirement for millimolar $Ca^{2+}$ in addition to RSOV energization was previously reported to stimulate $Mn^{2+}$ uptake in *E. coli* RSOV (42). Because MntH is the sole manganese uptake system known in *E. coli* laboratory strains, our data may suggest a possible link between MntH transport and external $Ca^{2+}$, which might be reminiscent of interactions between a DMT1 mutant and $Ca^{2+}$ (6). Strong asymmetry observed between MntH forward and reverse uptakes supports the proposition that MntH functions as a pump driven by $\Delta\psi$, accumulating cytosolic $Me^{2+}$ against their concentration gradient. Kinetic studies of $H^+$-coupled transport systems have shown that $\Delta\psi$ regulates $H^+$ binding or uptake, and that $H^+$ coupling increases a transporter affinity for its substrates or provides some thermodynamic force for the translocation step (2). Such a mechanism is widespread in microbes and was conserved in higher eukaryotic systems where an acid microclimate produces a huge proton gradient (*e.g.* the epithelial brush-border membrane of the proximal intestine, site of uptake by Nramp2 of non-heme dietary iron (58), and the phagosomal lumen in phagocytes that is depleted from $Me^{2+}$ by Nramp1 (59)). It is thus expected that future work on the *E. coli* MntH mechanism of the $H^+$-dependent transport will reveal additional structure-function relationships key to the Nramp/SLC11 family.

Evolutionary targeting of sites for biochemical analyses and three-dimensional validation of the results provides a framework to locate distinct TM residues key to the mechanism of the SLC11 membrane transport family. Low levels of sequence identity between SLC11 and SLC6 families (<20%) implies that the "LeuT-like" structural models obtained probably indicate a possibility that different families of cation transporters may share a general fold that could include inverted symmetry and discontinuous TM helices. SLC11 crystals will be required to ultimately validate any predicted model with resolution and accuracy. Nevertheless, the high resolution of the LeuT structure, which was corroborated by extensive biochemical and mutagenesis data, provided a high quality modeling template, and the suggested fit between the deduced architecture and SLC11 transporters topological and functional data imply that the current model holds significant potential for future studies of the SLC11 mechanism of $Me^{2+}/H^+$ symport and investigations of naturally occurring mutants in relation to diseases.

*Acknowledgments—We thank T. A. Tompkins for providing L. casei genomic DNA (R0215), T. Pugsley for supplying E. coli strain PAP3402, J. Beaubien for technical assistance, E. Narayanan for help with ModWeb analyses, P. Gros for support, and H. R. Kaback for critical comments.*

## REFERENCES


1. Cellier, M., Prive, G., Belouchi, A., Kwan, T., Rodrigues, V., Chia, W., and Gros, P. (1995) *Proc. Natl. Acad. Sci. U. S. A.* **92,** 10089–10093
2. Mackenzie, B., and Hediger, M. A. (2004) *Pflugers Arch.* **447,** 571–579
3. Cellier, M. F., Courville, P., and Campion, C. (2007) *Microbes Infect.* **9,** 1662–1670
4. Fortier, A., Min-Oo, G., Forbes, J., Lam-Yuk-Tseung, S., and Gros, P. (2005) *J. Leukocyte Biol.* **77,** 868–877
5. Nevo, Y., and Nelson, N. (2006) *Biochim. Biophys. Acta* **1763,** 609–620
6. Courville, P., Chaloupka, R., and Cellier, M. F. (2006) *Biochem. Cell Biol.* **84,** 960–978
7. Cheah, J. H., Kim, S. F., Hester, L. D., Clancy, K. W., Patterson, S. E., III, Papadopoulos, V., and Snyder, S. H. (2006) *Neuron* **51,** 431–440
8. Granseth, E., Seppala, S., Rapp, M., Daley, D. O., and von Heijne, G. (2007) *Mol. Membr. Biol.* **24,** 329–332
9. Lemieux, M. J. (2007) *Mol. Membr. Biol.* **24,** 333–341
10. Chaloupka, R., Courville, P., Veyrier, F., Knudsen, B., Tompkins, T. A., and Cellier, M. F. (2005) *Biochemistry* **44,** 726–733
11. Haemig, H. A., and Brooker, R. J. (2004) *J. Membr. Biol.* **201,** 97–107
12. Makui, H., Roig, E., Cole, S. T., Helmann, J. D., Gros, P., and Cellier, M. F. (2000) *Mol. Microbiol.* **35,** 1065–1078
13. Kehres, D. G., Zaharik, M. L., Finlay, B. B., and Maguire, M. E. (2000) *Mol. Microbiol.* **36,** 1085–1100
14. Courville, P., Chaloupka, R., Veyrier, F., and Cellier, M. F. (2004) *J. Biol. Chem.* **279,** 3318–3326
15. Daley, D. O., Rapp, M., Granseth, E., Melen, K., Drew, D., and von Heijne, G. (2005) *Science* **308,** 1321–1323
16. Kaback, H. R., Dunten, R., Frillingos, S., Venkatesan, P., Kwaw, I., Zhang, W., and Ermolova, N. (2007) *Proc. Natl. Acad. Sci. U. S. A.* **104,** 491–494
17. Chen, X., Peng, J., Cohen, A., Nelson, H., Nelson, N., and Hediger, M. A. (1999) *J. Biol. Chem.* **274,** 35089–35094
18. Sacher, A., Cohen, A., and Nelson, N. (2001) *J. Exp. Biol.* **204,** 1053–1061
19. Mackenzie, B., Ujwal, M. L., Chang, M. H., Romero, M. F., and Hediger, M. A. (2006) *Pflugers Arch.* **451,** 544–558
20. Gaucher, E. A., Gu, X., Miyamoto, M. M., and Benner, S. A. (2002) *Trends Biochem. Sci.* **27,** 315–321
21. Gu, X. (2006) *Mol. Biol. Evol.* **23,** 1937–1945
22. Madabushi, S., Gross, A. K., Philippi, A., Meng, E. C., Wensel, T. G., and Lichtarge, O. (2004) *J. Biol. Chem.* **279,** 8126–8132
23. Richer, E., Courville, P., Bergevin, I., and Cellier, M. F. (2003) *J. Mol. Evol.* **57,** 363–376
24. Grass, G., Franke, S., Taudte, N., Nies, D. H., Kucharski, L. M., Maguire, M. E., and Rensing, C. (2005) *J. Bacteriol.* **187,** 1604–1611
25. Quick, M., Tomasevic, J., and Wright, E. M. (2003) *Biochemistry* **42,** 9147–9152
26. Rensing, C., Fan, B., Sharma, R., Mitra, B., and Rosen, B. P. (2000) *Proc. Natl. Acad. Sci. U. S. A.* **97,** 652–656
27. Peterson, G. L. (1977) *Anal. Biochem.* **83,** 346–356
28. Zhang, W., and Kaback, H. R. (2000) *Biochemistry* **39,** 14538–14542
29. Cheng, H. C. (2001) *J. Pharmacol. Toxicol. Methods* **46,** 61–71
30. Matsushita, K., Inoue, T., Adachi, O., and Toyama, H. (2005) *J. Bacteriol.* **187,** 4346–4352
31. Laemmli, U. K. (1970) *Nature* **227,** 680–685
32. Blum, H., Beier, H., and Gross, H. J. (1987) *Electrophoresis* **8,** 93–99
33. Pieper, U., Eswar, N., Davis, F. P., Braberg, H., Madhusudhan, M. S., Rossi, A., Marti-Renom, M., Karchin, R., Webb, B. M., Eramian, D., Shen, M. Y., Kelly, L., Melo, F., and Sali, A. (2006) *Nucleic Acids Res.* **34,** D291–D295
34. Jones, D. T., Bryson, K., Coleman, A., McGuffin, L. J., Sadowski, M. I., Sodhi, J. S., and Ward, J. J. (2005) *Proteins* **61,** Suppl. 7, 143–151
35. Wu, S., and Zhang, Y. (2007) *Nucleic Acids Res.* **35,** 3375–3382
36. Shindyalov, I. N., and Bourne, P. E. (1998) *Protein Eng.* **11,** 739–747
37. Holm, L., and Park, J. (2000) *Bioinformatics* **16,** 566–567
38. Kawabata, T. (2003) *Nucleic Acids Res.* **31,** 3367–3369
39. Rahman, M., Ismat, F., McPherson, M. J., and Baldwin, S. A. (2007) *Mol. Membr. Biol.* **24,** 407–418
40. Liu, G., Hinch, B., Davatol-Hag, H., Lu, Y., Powers, M., and Beavis, A. D. (1996) *J. Biol. Chem.* **271,** 19717–19723
41. Lam-Yuk-Tseung, S., Govoni, G., Forbes, J., and Gros, P. (2003) *Blood* **101,** 3699–3707
42. Bhattacharyya, P. (1970) *J. Bacteriol.* **104,** 1307–1311
43. Robertson, D. E., Kaczorowski, G. J., Garcia, M. L., and Kaback, H. R. (1980) *Biochemistry* **19,** 5692–5702
44. Singh, S. K., Yamashita, A., and Gouaux, E. (2007) *Nature* **448,** 952–956
45. Bowie, J. U., Luthy, R., and Eisenberg, D. (1991) *Science* **253,** 164–170
46. Gunshin, H., Mackenzie, B., Berger, U. V., Gunshin, Y., Romero, M. F., Boron, W. F., Nussberger, S., Gollan, J. L., and Hediger, M. A. (1997) *Nature* **388,** 482–488
47. Cohen, A., Nevo, Y., and Nelson, N. (2003) *Proc. Natl. Acad. Sci. U. S. A.* **100,** 10694–10699
48. Arguello, J. M. (2003) *J. Membr. Biol.* **195,** 93–108
49. Dutta, S. J., Liu, J., Stemmler, A. J., and Mitra, B. (2007) *Biochemistry* **46,** 3692–3703
50. Su, C. C., Li, M., Gu, R., Takatsuka, Y., McDermott, G., Nikaido, H., and Yu, E. W. (2006) *J. Bacteriol.* **188,** 7290–7296
51. Hu, J., Fu, R., Nishimura, K., Zhang, L., Zhou, H. X., Busath, D. D., Vijayvergiya, V., and Cross, T. A. (2006) *Proc. Natl. Acad. Sci. U. S. A.* **103,** 6865–6870
52. Larsen, R. A., Deckert, G. E., Kastead, K. A., Devanathan, S., Keller, K. L., and Postle, K. (2007) *J. Bacteriol.* **189,** 2825–2833
53. Pornillos, O., and Chang, G. (2006) *FEBS Lett.* **580,** 358–362
54. Screpanti, E., and Hunte, C. (2007) *J. Struct. Biol.* **159,** 261–267
55. Zhou, F. X., Cocco, M. J., Russ, W. P., Brunger, A. T., and Engelman, D. M. (2000) *Nat. Struct. Biol.* **7,** 154–160
56. Likitvivatanavong, S., Katzenmeier, G., and Angsuthanasombat, C. (2006) *Arch. Biochem. Biophys.* **445,** 46–55
57. Liu, K., Kozono, D., Kato, Y., Agre, P., Hazama, A., and Yasui, M. (2005) *Proc. Natl. Acad. Sci. U. S. A.* **102,** 2192–2197
58. Thwaites, D. T., and Anderson, C. M. (2007) *Exp. Physiol.* **92,** 603–619
59. Martin-Orozco, N., Touret, N., Zaharik, M. L., Park, E., Kopelman, R., Miller, S., Finlay, B. B., Gros, P., and Grinstein, S. (2006) *Mol. Biol. Cell* **17,** 498–510
60. DeLano, W. L. (2005) *Drug Discov. Today* **10,** 213–217